

A feasibility study of photosensor charge signal transmission to preamplifier using long cable for development of hybrid PET-MRI

Jihoon Kang, Yong Choi,^{a)} Key Jo Hong, Jin Ho Jung, Wei Hu, Yoon Suk Huh, and Hyunkeong Lim

Department of Electronic Engineering, Sogang University, 1 Shinsu-Dong, Mapo-Gu, Seoul 121-742, Republic of Korea and Department of Nuclear Medicine, Samsung Medical Center, Sungkyunkwan University School of Medicine, 50 Ilwon-Dong, Gangnam-Gu, Seoul 135-710, Republic of Korea

Byung-Tae Kim

Department of Nuclear Medicine, Samsung Medical Center, Sungkyunkwan University School of Medicine, 50 Ilwon-Dong, Gangnam-Gu, Seoul 135-710, Korea

(Received 22 April 2010; revised 8 September 2010; accepted for publication 8 September 2010; published 8 October 2010)

Purpose: A new positron emission tomography (PET) detector signal processing method, the charge signal transmission approach, is proposed for the development of a hybrid PET-magnetic resonance imaging (MRI). A number of experiments were performed to demonstrate that the Geiger-mode avalanche photodiode (GAPD) charge output could be transmitted to a preamplifier using a long cable without degrading the PET signal performance.

Methods: A PET module consisted of LYSO and a GAPD with a 4×4 array. The GAPD output was transmitted to the preamplifier through flexible flat cables. The effect of the cable length on the PET performance was examined using seven different lengths ranging from 10 to 300 cm outside and inside the 7 T animal MRI. Four parameters (rise time, fall time, amplitude, and area of the preamplifier output) were measured as a function of the cable length using a 10 GS/s oscilloscope and three parameters (photopeak position, energy resolution, and time resolution) were measured using a 100 MS/s DAQ unit. The effect of the cable length on the MR phantom images was investigated. In addition, the effect of the PET module configuration on its temperature stability was assessed by acquiring the energy and time spectra.

Results: There were no significant changes in the PET module performance as a function of the cable length, both outside and inside MRI. The performance changes in energy information, such as the amplitude, area, photopeak position, and energy resolution, were $<3\%$ with cable lengths ranging from 10 to 300 cm and the change in the time resolution was $<6\%$. There were no obvious artifacts or changes in the line profile in the MR phantom images. Moreover, no manifest changes in the photopeak position and coincidence counting rate were observed in the PET modules employing the charge signal transmission approach, whereas considerable degradation of the PET module performance was observed in the voltage signal transmission approach.

Conclusions: This study demonstrated that it is feasible to design a hybrid PET-MRI using the charge signal transmission approach, which is expected to have more advantages than other approaches. © 2010 American Association of Physicists in Medicine. [DOI: 10.1118/1.3495683]

Key words: hybrid PET-MRI, charge signal transmission, Geiger-mode avalanche photodiode (GAPD), flexible flat cables (FFCs), mutual interference between PET and MRI

I. INTRODUCTION

There has been considerable interest in the development of multimodal imaging systems that can supplement the weak points of individual systems and provide more comprehensive biological and diagnostic information.^{1,2} In 1998, a combined positron emission tomography (PET)/CT scanner was introduced for molecular and morphological imaging and has rapidly become an important diagnostic tool in nuclear medicine over the past decade.^{3,4} However, the current version of PET/CT can acquire only sequential images, which makes it difficult to obtain accurately registered images and temporal correlation between two image sets. As an alternative, a combined PET-magnetic resonance imaging (MRI) can produce isocentric and simultaneous images. MRI provides excellent

soft tissue contrast without the need for an additional radiation dose compared to CT.^{5,6} In addition, a hybrid PET-MRI for clinical use could provide more diagnostic information in brain studies than PET/CT.⁷

However, certain technical challenges caused by the high magnetic field environment need to be solved when combining PET and MRI. The major issues are whether potential mutual interference between two modalities can be minimized and whether the individual components can be operated without degrading performance. There are several approaches for designing a MRI-compatible PET system that can overcome various technical challenges and can be classified according to the transmission method of the PET signal from inside the MR bore to outside of it.

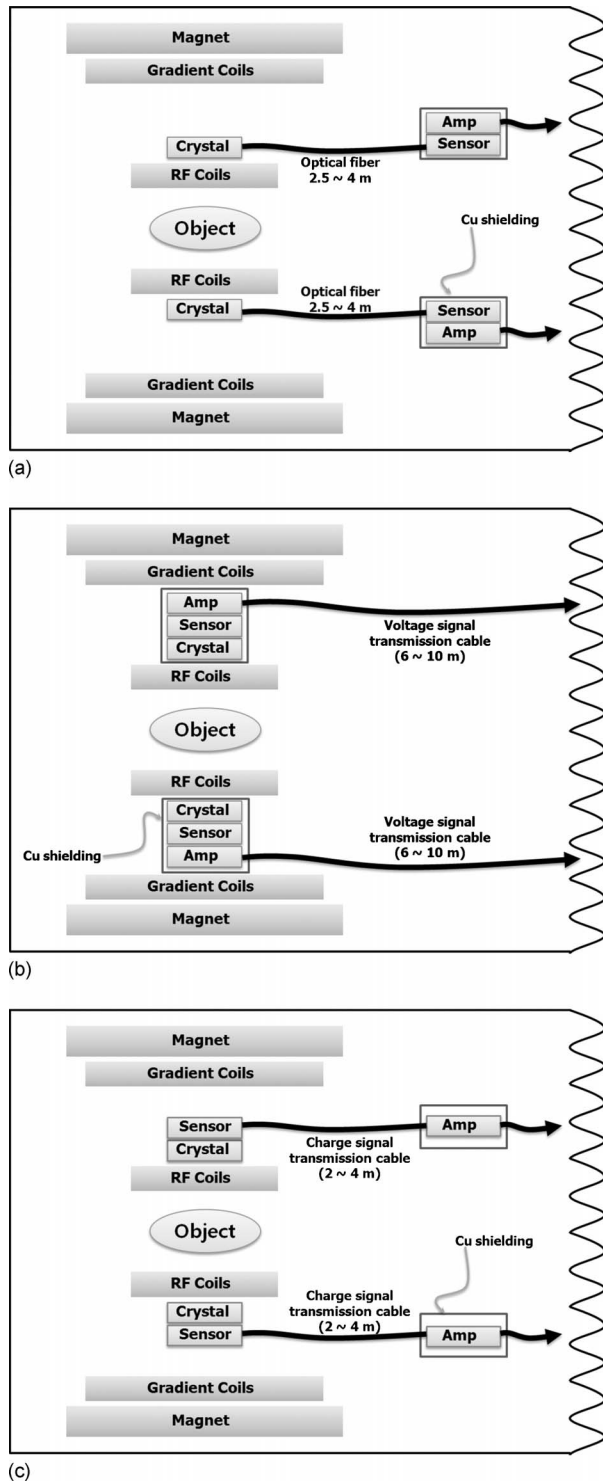


FIG. 1. Several approaches for designing hybrid MR compatible PET. (a) Approach 1: Scintillation light transmission from crystal to photosensor. (b) Approach 2: Voltage signal transmission from amplifier to subsequent electronics. (c) Approach 3: Charge signal transmission from photosensor to preamplifier.

The first approach transmits the scintillation light generated in a scintillation crystal using optical fibers to photosensors, such as a photomultiplier tube (PMT). In this case, the crystal is placed inside the MR bore and the photosensor and amplifier circuit are placed outside [Fig. 1(a)].⁸⁻¹¹ However,

this approach has serious drawbacks that degrade the PET performance, such as the energy and time resolution due to the loss and dispersion of scintillation light by the optical fibers. In addition, it is difficult to extend the axial field of view without major modifications of the magnet design and the optical fibers are too fragile and bulky making it difficult to construct such a system.

The second approach is that the PET signals amplified in a preamplifier are transmitted to the ADC or other subsequent signal processing circuits using voltage transmission cables. In this case, the PET modules consisting of a scintillation crystal, photosensor, and signal amplifying circuits are placed inside the MR bore [Fig. 1(b)]. Such systems have been constructed and are currently under investigation by most hybrid PET-MRI research groups.¹²⁻¹⁴ Using this approach, it is necessary (essential) to locate the front-end electronics including the preamplifier, channel reduction electronics, etc., as well as the scintillation crystal and photosensor inside the MR bore, which has limited space. It also requires careful shielding of the inserted PET modules to protect it from electromagnetic interference. Moreover, eddy current can be generated in a conducting material, such as PET shielding and amplifier circuit board, which might distort the MRI, reduce the effective gradient strength, and generate heat inside the shielding material.⁵

The third approach, which is proposed in this work, is that the charge signal of the photosensor is transmitted to the preamplifier through charge transmission cables. In this case, the crystal and photosensor are placed inside the MR bore and the PET signal is transmitted to the signal amplifier circuits located outside the MR bore using a long cable [Fig. 1(c)]. Generally, this approach has not been considered for the development of PET. The preamplifier needs to be mounted as close as possible to the photosensor to minimize noise because the photosensor output is a weak charge signal and the equivalent noise charge (ENC) is proportional to the input capacitance of the preamplifier.¹⁵

With the advent of the Geiger-mode avalanche photodiode (GAPD), which provides high gain, high photodetection efficiency, and low noise, it might be possible to transmit the GAPD charge output to the preamplifier using a long cable without degrading the PET data performance. The GAPD provides high charge amplitudes at the output and can maintain a relative high signal to noise ratio (SNR), even with a high noise source. In addition, a range of compact cables with relatively small capacitance and high characteristic impedance that can avoid the excessive increase in ENC value have been introduced, facilitating the charge signals transmission through a long cable.

The aim of this study was to examine if approach 3 could be used to design a hybrid PET-MRI system and to evaluate the merits of this approach compared to others. A number of experiments were performed to demonstrate that the GAPD charge output could be transmitted to a preamplifier using a long cable without degrading the PET signal performance. An additional study was performed to determine if the PET

modules constructed by approaches 2 [Fig. 1(b)] and 3 [Fig. 1(c)] could be operated without the degradation caused by heat generation by the amplifier circuits.

II. MATERIALS AND METHODS

II.A. Experiment materials

II.A.1. PET detector modules

Each PET detector consisted of a lutetium yttrium oxyorthosilicate (LYSO) array (Sinocera, Shanghai, China), which contained 4×4 individual $3 \times 3 \times 20$ mm crystals arranged with a 3.3 mm pitch. The crystal pixels were polished on all faces and separated by white epoxy except for the surface facing the photosensor [Fig. 2(a)]. The LYSO crystal has excellent properties, such as high stopping power for the annihilation photons (linear attenuation coefficient $= 0.86 \text{ cm}^{-1}$), high light output ($\sim 12\,775$ photons/511 keV), fast decay time (~ 40 ns), and low cost. In addition, it has a similar magnetic susceptibility to human tissue and may be suitable for fabricating a MR compatible PET.^{16,17}

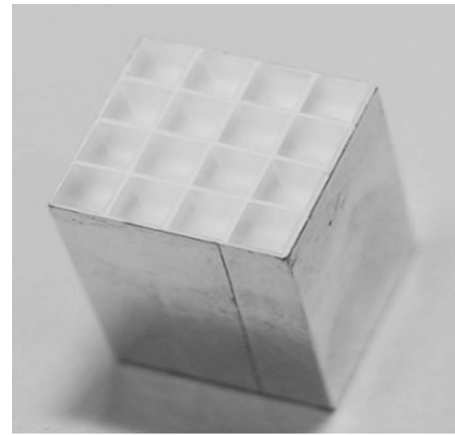
A three-sided buttable GAPD array, which makes it possible to configure a PET ring system with minimized dead space, was used for the scintillation light readout. The 4×4 GAPD arrays (SensL, Cork, Ireland) consisted of 3×3 mm pixels with 3640 microcells arranged with a pitch of 3.3 mm [Fig. 2(b)]. GAPD was reported to have many advantages, such as high gain, low voltage operation, insensitivity to magnetic fields, and sufficient dynamic range for 511 keV annihilation radiations.^{18,19} Table I lists the properties of the GAPD arrays used in this study. An individual LYSO crystal was coupled one to one to a separate pixel of the GAPD without optical grease. The black tape was applied as a shield from light [Fig. 2(c)].

The flexible flat cables (FFCs) (New Grand TECH, Shenzhen, China) were used to transmit the charge signal from the GAPD to remotely located preamplifiers. The FFCs have good properties suitable to bond to a cable connector on a compactly designed GAPD, to transmit the multichannel GAPD output signals, and to supply the low bias voltage to GAPD (~ 32 V) without a voltage drop. Also, these have relatively low capacitance (33.6 pF/m) to avoid an increase in the ENC that can occur in long cable runs. Crosstalk between signal lines of the FFCs was improved using a ground-signal-ground configuration in which each signal line runs between ground lines.

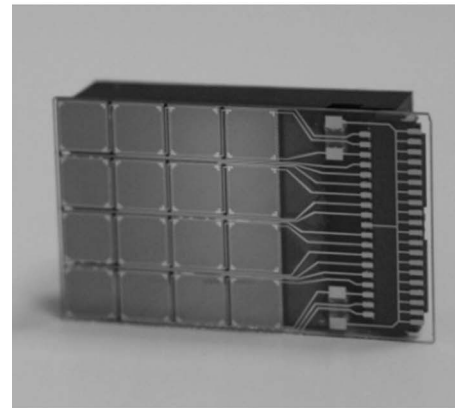
II.A.2. Amplifier and data acquisition system

The transimpedance preamplifiers were used to efficiently convert the charge transmitted by the long cable into the amplified voltage signal. The amplifier unit used in this study includes the voltage regulation circuit which makes it possible to finely adjust the bias voltage using a digital potentiometer and provide optimal bias conditions for GAPD.

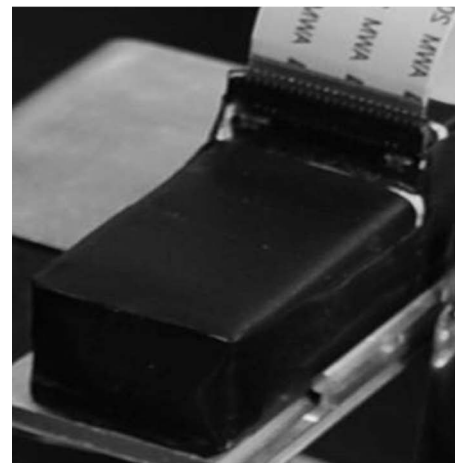
The amplified voltage signals were fed into the 14-bit free-running ADCs with a 105 MHz clock in the -1.25 to $+1.25$ V range. The digitized signals were then processed using a field programmable gate array board implemented to



(a)



(b)



(c)

FIG. 2. Images of the PET detector components: (a) LYSO crystal, (b) GAPD array, and (c) PET detector shielded from light.

calculate the energy and timing information for each gamma ray.²⁰ After signal processing, the output data containing the pulse energy, arrival time, and position information were recorded on 128 MB SDRAM, which has a data transfer bandwidth of 450 MB/s. The list-mode format data were processed further to apply a lower level discriminator, upper level discriminator, and coincidence timing window.

TABLE I. Specifications of the three-sided buttable GAPD arrays used in this study.

Parameter	Properties
Gain	$\sim 1 \times 10^6$
Active area of individual pixel	$2.85 \times 2.85 \text{ mm}^2$
Microcell size of individual pixel	$35 \times 35 \text{ }\mu\text{m}^2$
Microcell numbers of individual pixel	3640
Bias voltage	$\sim 28.5 \text{ V}$
PDE ^a at 420 nm, 4 V above V_{Bias}	$\sim 15\%$
Fired pixels at 511 keV, LYSO	1705

^aPDE: Photon detection efficiency.

II.B. Experimental methods

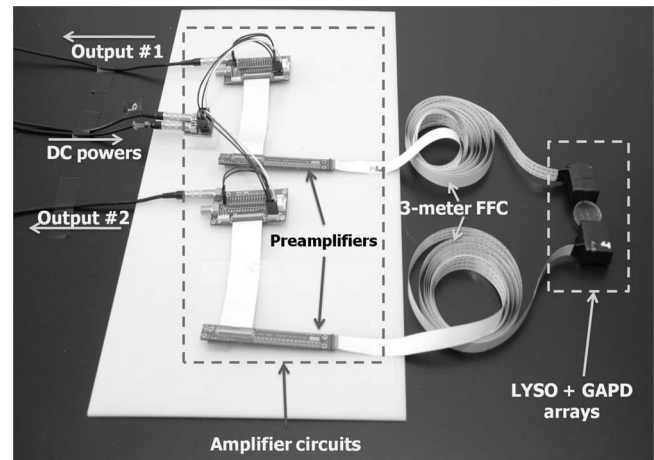
II.B.1. Performance measurement as a function of cable length outside MRI

A pair of fully assembled PET modules were tested outside the MRI as the cable length between GAPD and preamplifier was changed [Fig. 3(a)]. The measurement data were acquired by exposing the crystal arrays to a 200 kBq ^{22}Na point source, which was located between a pair of detector modules. The two types of DC power supplies were used to bias the GAPD arrays (+32 V) and operate the preamplifiers (+5.2 V). The output of the preamplifier was fed into the oscilloscope or data acquisition (DAQ) system without an additional shaping amplifier.

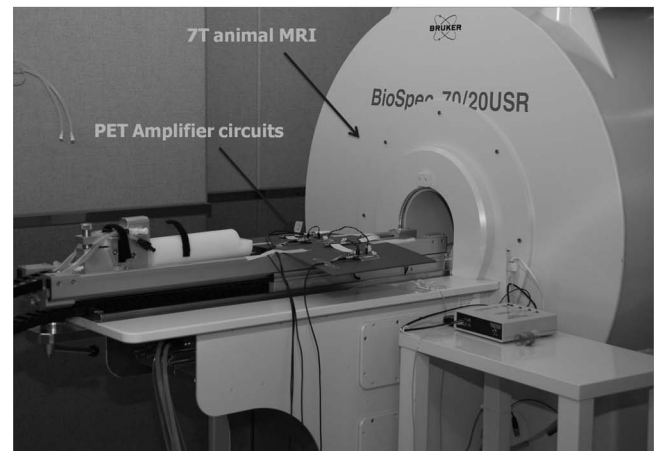
The effect of the cable length was examined for seven different lengths ranging from 10–300 cm. The following four parameters were measured using a 10 GS/s oscilloscope: Rise time, fall time, amplitude, and area of the preamplifier output. The pulse data were acquired over 10 000 counts to reduce the statistical uncertainty ($<1\%$). In addition, the following three parameters were measured using a DAQ unit: Photopeak channel of the 511 keV, energy resolution, and timing resolution. The experimental tests were repeated three times at 26 °C to examine the reproducibility of the results, which could be caused by imprecise measurements by random error, gain variations of the GAPD array due to temperature changes, and electronic noise for a given photosensor or preamplifier. The temperature of the PET detector modules was stabilized to room temperature using a cooling fan and monitored throughout the measurements by a micro-processor based digital thermometer.

II.B.2. Performance measurement as a function of cable length inside MRI

The performance of the PET module was also measured and recorded inside the MR bore to examine the MR compatibility as a function of the cable length. The experiment was performed on a 7 T animal MRI (Bruker, Ettlingen, Germany) using a RF-coil set with a 34 mm inner diameter/59 mm outer diameter [Fig. 3(b)]. The LYSO-GAPD PET detector modules were inserted inside the MR bore between the RF coil and gradient coil, whereas the preamplifiers were positioned outside the MR bore. The DC power was supplied by a 10 m long cable into the MRI room. The preamplifier



(a)



(b)

Fig. 3. Experimental setup to examine the effect of the cable length on both PET and MRI. (a) PET detector performance measurement outside MRI. A pair of PET detector modules was exposed by Na-22 point source and PET charge signals were transmitted to the preamplifier using FFC of 300 cm. (b) PET performance measurement inside the MRI. The PET detector modules were inserted into the MR bore between the RF coil and gradient coil (not displayed), while the preamplifier is located outside the MR bore ($<5 \text{ G line, } \sim 1.5 \text{ m}$ away from the magnet isocenter).

output signals, which were connected to the oscilloscope and DAQ board, were transmitted to outside the MRI room via 5 m long cable. The trans-axial images of a CuSO_4 -filled phantom were acquired using gradient echo (GE) ($\text{TR}=205 \text{ ms, TE}=6 \text{ ms, and FA}=15^\circ$), spin echo T1 (SE.T1) ($\text{TR}=419 \text{ ms and TE}=8 \text{ ms}$), and spin echo T2 (SE.T2) ($\text{TR}=3000 \text{ ms and TE}=75 \text{ ms}$) sequences.

II.B.3. Effect of PET module configuration on its temperature stability

Two types of PET detector modules were constructed to examine the effect of heat generation by the preamplifiers. One is that all components of the PET module, including the LYSO, GAPD arrays, and preamplifiers, were located in an integrated housing box [Fig. 4(a)], which resembled the voltage signal transmission approach to design a hybrid PET-MRI [Fig. 1(b)]. The other is that the LYSO and GAPD

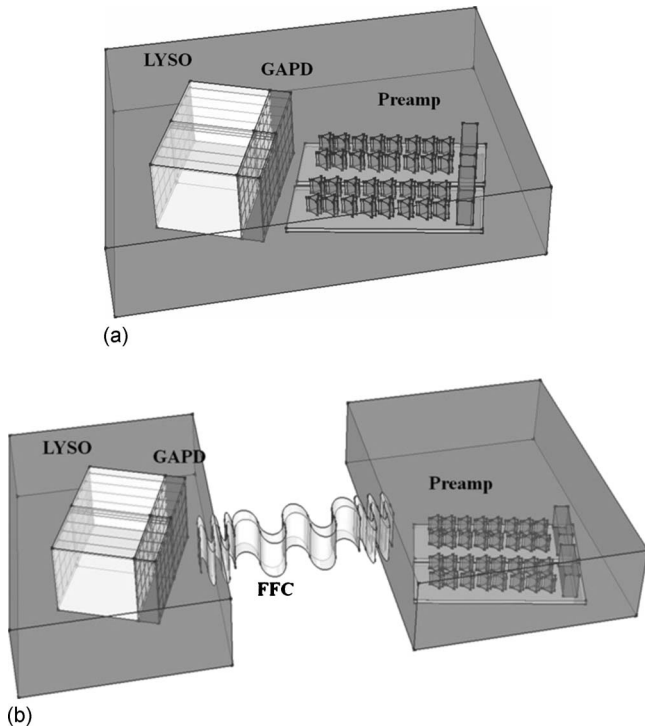


FIG. 4. Schematic diagram of the two types of PET detector modules to examine the temperature stability. (a) The LYSO, GAPD, and preamplifiers were located in the integrated housing box similar to approach 2 [Fig. 1(b)]. (b) PET detectors and preamplifiers were positioned in a separated housing box simulating approach 3 [Fig. 1(c)].

arrays were located without the preamplifiers in the plastic box [Fig. 4(b)], which is similar to the charge signal transmission approach [Fig. 1(c)]. The GAPD array and preamplifiers were connected using a 30 cm FFC cable and the data including the temperatures, energy, and time spectra were obtained at 10 min intervals for 1 h for each configuration.

III. RESULTS

III.A. Performance measurement as a function of cable length outside MRI

Figure 5 shows representative output waveforms of the preamplifier, which were measured using 10 and 300 cm cables. Visually, the pulse amplitude was independent of the

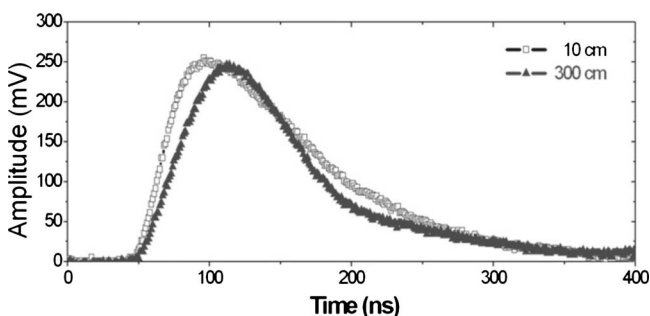


FIG. 5. Representative output waveform of the preamplifier. The rise time obtained using the 300 cm cable (\blacktriangle) was noticeably slower than the one obtained using the 10 cm cable (\square).

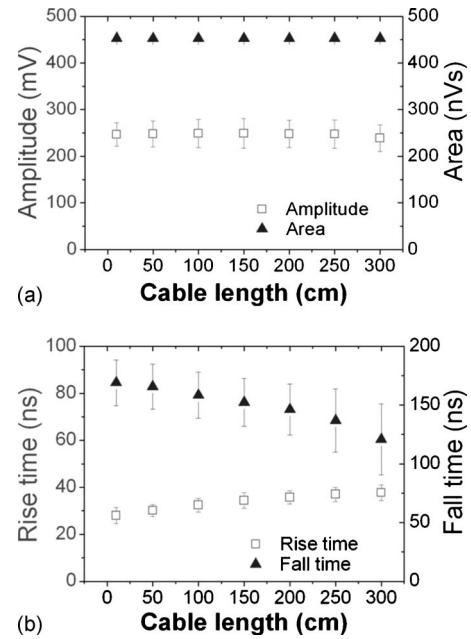


FIG. 6. PET detector performance as a function of the cable length. (a) The changes in amplitude (\square) and area under the pulse (\blacktriangle) obtained as a function of the cable length, 10–300 cm. (b) The changes in the rise time (\square) and fall time (\blacktriangle) obtained as a function of the cable length, 10–300 cm.

cable length and no unexpected noise sources, such as time jitter, baseline shift, and pulse oscillation, were observed with the long cables. However, time information, such as the rise time, fall time, and peaking time, changed considerably depending on the cable length used.

Figure 6(a) shows the amplitude (left) and area (right) of the preamplifier outputs as a function of the cable length. The coefficient of variation was $<2\%$ for the amplitude and $<1\%$ for the area obtained with cables of different lengths from 10 to 300 cm. Each point is an average of at least 10 000 pulse measurements at each cable length and the error bar is the standard deviation. Figure 6(b) shows the rise time (left) and fall time (right) of the preamplifier output as a function of the cable length. The rise time increased from 28 to 38 ns with increasing cable length and the fall time decreased from 169 to 120 ns. One possible cause is that the rise time increased with increasing input capacitance in the time response of a preamplifier.²¹ In addition, the total capacitance increased with increasing cable length and high frequency elements of the GAPD output were filtered by the additional cable capacitance which caused a slow rise time and short fall time.

Figure 7 shows the energy and timing spectra measured using 10 and 300 cm cables. There was no noticeable degradation in the PET detector module performance observed using the long cable (300 cm) from the GAPD to the preamplifier in the PET signal transmission. The Gaussian function fitted to the data had a FWHM of $\sim 20\%$ and ~ 1.7 ns, respectively. Note that the energy resolution was relatively poor,^{22,23} partly due to the coupling crystal to the GAPD array without optical grease.

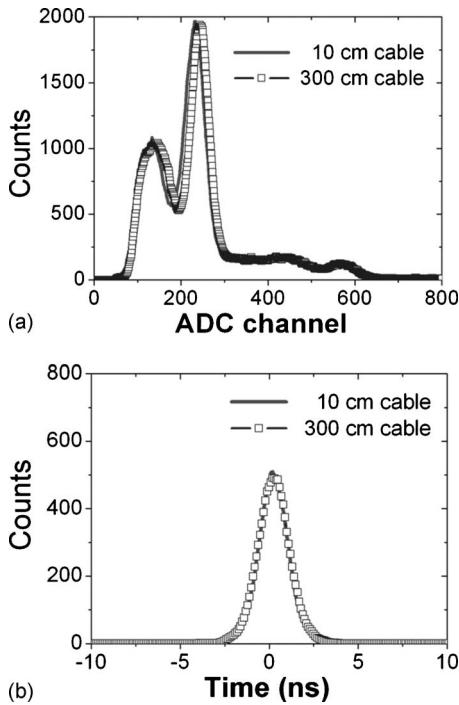


FIG. 7. (a) Representative energy and (b) time spectra of the PET detector acquired with a 10 cm (—) and 300 cm cable (□)

Figure 8(a) shows the changes in the photopeak channel and energy resolution as a function of the cable length in the energy spectra. The photopeak position and energy resolution of the 511 keV varied with a coefficient of variation of 2.2% and 1.1%, respectively. Figure 8(b) shows the changes in the time resolution as function of the cable length in the

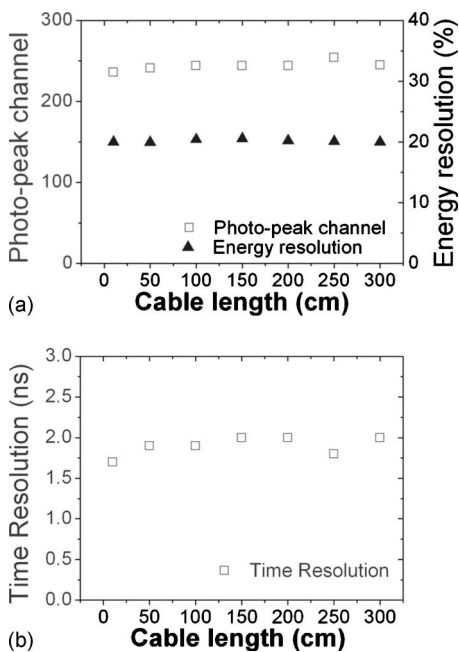


FIG. 8. PET detector performance as a function of the cable length. (a) The changes in the photopeak channel (□) and energy resolution (▲) measured with different cable lengths, 10–300 cm. (b) The changes in time resolution (□) measured with different cable lengths, 10–300 cm.

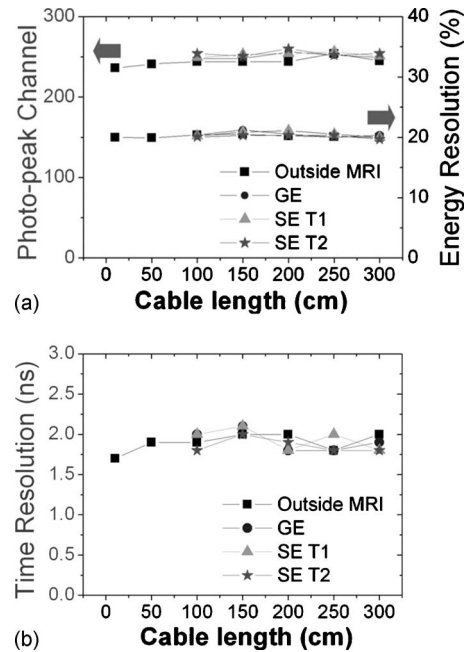


FIG. 9. The changes in PET detector performance as a function of the cable length measured inside the MRI. (a) The energy and (b) time information of the PET detector with seven different cable lengths were acquired using no sequence (■), GE (●), SE.T1 (▲), and SE.T2 (*) MR imaging sequences.

timing spectra. The maximum change was ~ 0.3 ns, which corresponds to a coefficient of variation of 6%.

III.B. Performance measurement as a function of cable length inside MRI

The trends in the energy and time information measured inside the MRI were similar to the results measured outside the MRI. No considerable changes in PET performance were observed in the MR environment. Figure 9 presents the performance results of the PET module while running the MR sequences.

Figure 10 shows the MR phantom images and line profiles acquired with and without the PET detector module located in the isocenter. ROI analysis revealed a respective SNR of 148 and 143 and a uniformity of 97.6 and 97.2. No obvious artifacts or changes in the line profiles were observed after inserting the PET module.

III.C. Effect of PET module configuration on its temperature stability

Figure 11 presents the energy and time spectra acquired with the PET detector module located in an integrated housing box, which might be used in the voltage signal transmission approach to design a hybrid PET-MRI [Fig. 1(b)]. Some changes in energy and time resolution were observed and serious alterations occurred in the photopeak position and coincidence counting rate due to the decreasing gain of the GAPD array caused by the increase in temperature in the plastic box. The temperature increased from room temperature (26°C) to 33°C after 1 h. In contrast, no considerable changes in temperature or performance of the PET module

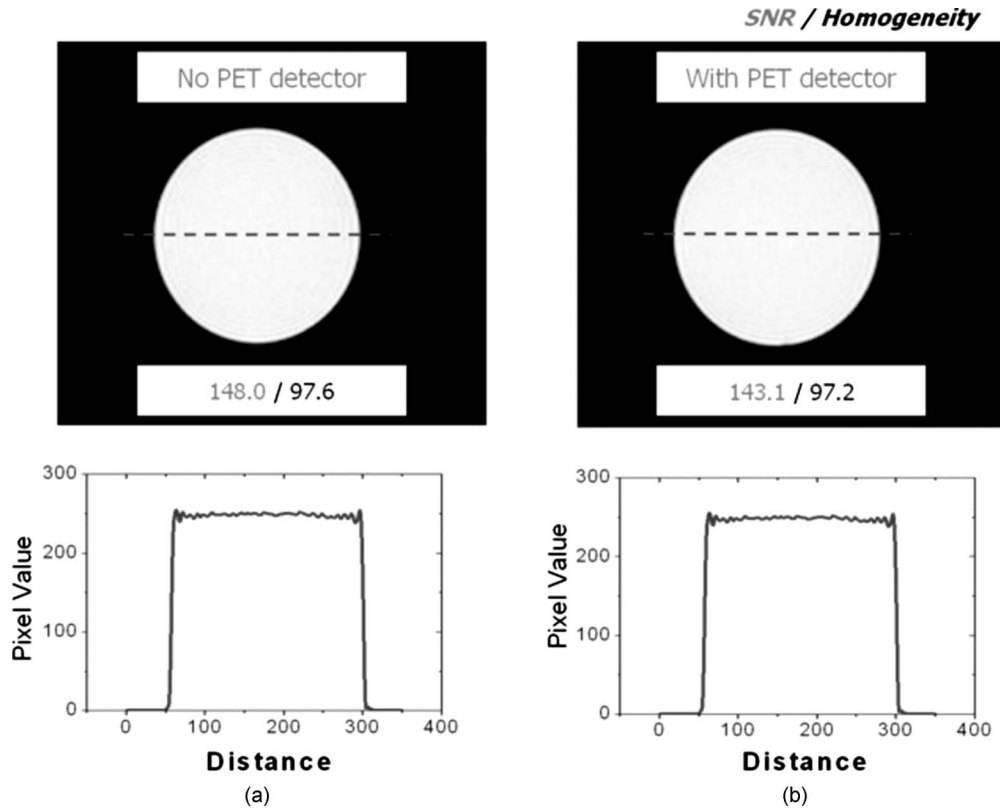


FIG. 10. Acquired MR phantom images and line profiles (a) without and (b) with the PET detector in the GE sequence (TR=205 ms, TE=6 ms, FA=15°).

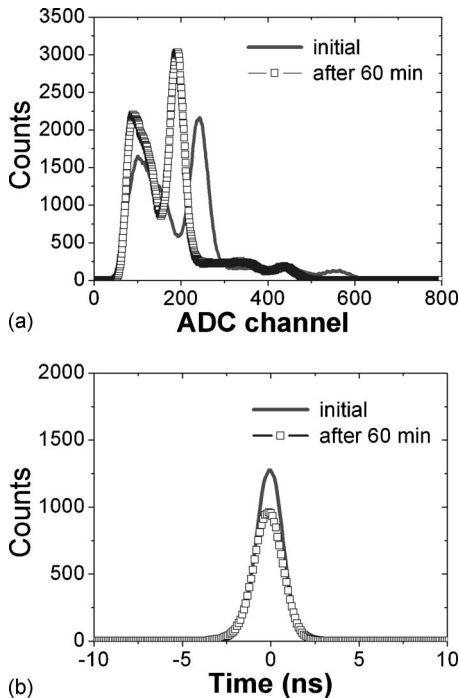


FIG. 11. (a) The energy and (b) time spectra of the PET module fabricated in the integrated housing box. The temperature of the housing box was increased from 26 up to 33 °C after 1 h.

were observed (Fig. 12) when the LYSO and GAPD array was located without a preamplifier in the plastic box, which bore close resemblance to the charge signal transmission approach [Fig. 1(c)].

The temperature changes resulted from the heat generated in the preamplifier, which radiated to the periphery. Figure 13 shows the changes in the performance of the PET detector modules fabricated in the integrated housing box (a) and separate housing box (b) as a function of the time elapsed.

IV. DISCUSSION

This study examined the feasibility of the charge signal transmission approach in the development of a hybrid PET-MRI. The PET detector module was operated with different cable lengths to determine if the charge output of the GAPD could be transmitted to a preamplifier using a long cable without degrading the PET performance. Seven parameters of the PET detector module (pulse amplitude, pulse area, rise time, fall time, photopeak position, energy resolution, and time resolution) were examined outside and inside the MRI. The measurement results showed two trends. One trend revealed <3% changes in energy information from the 10 to 300 cm cables, including the amplitude, area, photopeak position, and energy resolution [Figs. 6(a) and 8(a)]. This was attributed to the use of specific cables with relatively high characteristic impedance that could avoid the considerable increase in ENC values, even though the charge signal was transferred via the long cable.

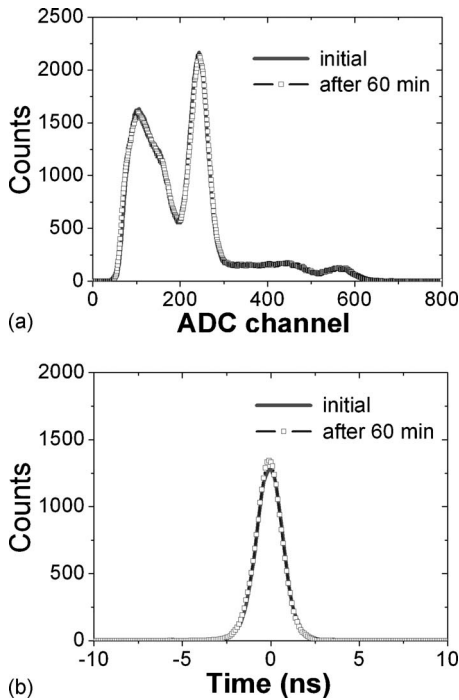


FIG. 12. (a) The energy and (b) time spectra of the PET module fabricated in the separated housing box. The temperature of the housing box with the PET detector was unchanged.

Another trend indicated a considerable change in time information, such as the rise time and fall time of the preamplifier output from the detectors with 10–300 cm cables [Fig. 6(b)]. These changes in preamplifier output were attributed to the additional input capacitance caused by the longer cable. However, the maximum change in the rise time, 10 ns,

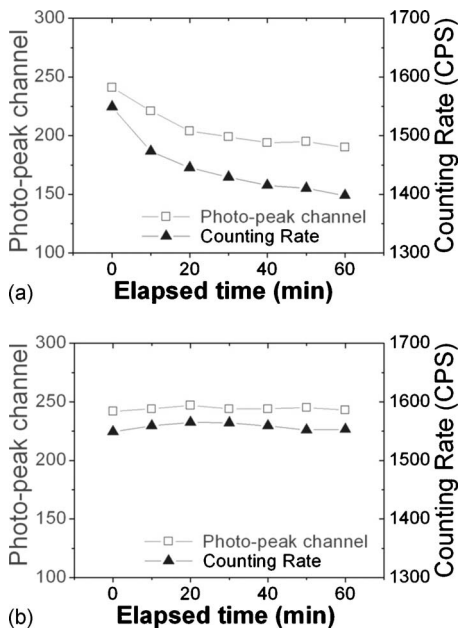


FIG. 13. Change in performance of the PET detector modules fabricated in the (a) integrated housing box and (b) separated housing box as a function of the elapsed time. Each data point was obtained at 10 min intervals for 1 h for each configuration.

was not a critical issue in generating a time mark for the coincidence detection in a test setup that employed the DAQ system with a 100 MHz ADC sampling rate (=10 ns sampling period). In this study, the maximum change in the time resolution from 10 to 300 cm was <0.3 ns [Fig. 8(b)]. These two trends of the PET detector performance were similar both outside and inside the MR environment (Fig. 9). No mutual interference of both modalities was observed even though the PET and MR data had been acquired simultaneously by inserting the PET detector between the gradient coil and RF coil.

Some studies of the charge signal transmission approach have been previously carried out to develop a nuclear application system albeit with moderate success. In the case of an idealized PMT output, Brianti²⁴ performed numerical analysis as a function of the coaxial cable type and length. He showed that a long cable deteriorated the PMT output, rise time, fall time, and amplitude significantly. Another assessment was performed by Despres *et al.*²⁵ for an evaluation of a MR compatible CdZnTe (CZT) detector. The experiment was carried out with a 1 m long coaxial cable between the CZT detector and preamplifier. Their results showed that the energy resolution of the CZT detector had degraded by more than 50% by introducing a 1 m long cable.

Although previous studies showed that the use of a long cable from the photosensor to preamplifier affects the detector performance, it could be attributed to the use of inappropriate long cables with low characteristic impedance and high capacitance. As described above, the low characteristic impedance generated impedance mismatch between the GAPD and cable and the high capacitance caused an increase in the ENC value. Since this study used a FFC with a relatively high characteristic impedance and low capacitance, no considerable degradation in PET detector performance was observed using this cable.

Considering that the axial range from the isocenter to the end-point in a MR bore is ~ 1 m, it is possible to develop a MR compatible PET system using the 300 cm FFC [approach 3, (Fig. 1(c))] because PET electronics could be located further away from the PET detector and MR isocenter. A MR compatible human brain and animal PET scanner using approach 3 [Fig. 1(c)] is currently under construction in our laboratory. Approach 3 should provide several potential merits for developing a hybrid PET-MRI compared to other approaches.

First, approach 3 [Fig. 1(a)] will allow the scalable design of hybrid PET-MRI, which makes it possible to insert a compact, slim, and lightweight PET scanner inside the MR bore compared to approaches 1 and 2 [Figs. 1(b) and 1(c)]. This is because in this configuration, only a crystal and GAPD array are inserted inside the MR bore without an optical fiber or preamplifier circuit to integrate a hybrid PET-MRI. In addition, the multichannel PET output signals in approach 3 are transmitted using a multicore slimline flexible ribbon cable, not a bulky coaxial cable or twist paired cable. Furthermore, it is relatively easy to bend and modify the signal transmission cables to fit the shape of the PET gantry.

Second, approach 3 does not result in a deterioration of

the PET performance. For example, the optical fibers partially absorb the scintillation light resulting in a degradation of the energy and time resolution.^{10,11} As shown in Figs. 11 and 13, the integrated housing of the GAPD and preamplifier resulted in a shift in the photopeak position and a decrease in the coincidence counting rate caused by increases in temperature while supplying the preamplifier power. Currently, several hybrid PET-MRI research groups based on semiconductor detectors have attempted to introduce a cooling system for stable PET operation.^{14,26,27} However, this problem can be avoided easily in approach 3 using a separate housing for the GAPD and preamplifier. Moreover, the heat generated by eddy currents can be minimized in approach 3.

Finally, approach 3 makes it possible to produce a cost-effective hybrid PET-MRI system. In approach 2, a low noise integrated preamplifier and effective RF shielding technique is needed.^{5,13} In addition, approach 1 requires the introduction of an effective attaching technique between crystal and optical fiber.¹⁰ On the other hand, a hybrid PET-MRI can be designed easily using approach 3 without integrated amplifier circuits, effective RF shielding, and fiber attaching techniques.

However, approach 3 also has a number of features that may render its implementation difficult. First, it requires a high gain photosensor to maintain the high SNR of the charge signal output. Second, it would be difficult to construct a time of flight PET scanner due to the increased pulse rise time, even though there is little change in time resolution when a 100 MHz ADC sampling rate in the DSP unit is used to generate a time mark.

V. CONCLUSIONS

This study examined the feasibility of transmitting the GAPD charge output to a preamplifier using a long cable. No considerable change in PET detector performance, both outside and inside the MRI, and no obvious artifacts or changes in the line profile caused by PET charge signal transmission using a long cable were observed in the MR phantom images. These results demonstrate that a hybrid PET-MRI can be designed using the charge signal transmission approach. Moreover, the charge signal transmission approach has potential advantages in the development of a hybrid PET-MRI without performance deterioration in both modalities.

ACKNOWLEDGMENTS

This study was supported by the Converging Research Center Program through the Ministry of Education, Science and Technology (Grant No. 2010K001109) and by the Technology Innovation Program through the Ministry of Knowledge Economy, Republic of Korea.

^{a)} Author to whom correspondence should be addressed. Electronic mail: ychoi.image@gmail.com

¹ K. J. Hong, Y. Choi, S. C. Lee, S. Y. Lee, T. Y. Song, B. J. Min, J. H. Jung, Y. S. Choe, K. H. Lee, and B. T. Kim, "A compact SPECT/CT system for small animal imaging," *IEEE Trans. Nucl. Sci.* **53**, 2601–2604 (2006).

² J. H. Jung, Y. Choi, K. J. Hong, B. J. Min, J. Y. Choi, Y. S. Choe, K.-H. Lee, and B.-T. Kim, "Development of a dual modality imaging system: A

combined gamma camera and optical imager," *Phys. Med. Biol.* **54**, 4547–4559 (2009).

³ T. Beyer, D. W. Townsend, T. Brun, P. E. Kinahan, M. Charron, R. Roddy, J. Jerin, J. Young, L. Byars, and R. Nutt, "A combined PET/CT scanner for clinical oncology," *J. Nucl. Med.* **41**, 1369–1379 (2000).

⁴ G. Brix, U. Lechel, G. Glatting, S. I. Ziegler, W. Munzing, S. P. Muller, and T. Beyer, "Radiation exposure of patients undergoing whole-body dual-modality F-18-FDG PET/CT examinations," *J. Nucl. Med.* **46**, 608–613 (2005).

⁵ B. J. Pichler, H. F. Wehrl, and M. S. Judenhofer, "Latest advances in molecular imaging instrumentation," *J. Nucl. Med.* **49**, 5S–23S (2008).

⁶ G. K. von Schulthess and H. P. Schlemmer, "A look ahead: PET/MR versus PET/CT," *Eur. J. Nucl. Med. Mol. Imaging* **36**, S3–S9 (2009).

⁷ D. Pauleit, F. Floeth, K. Hamacher, M. J. Riemenschneider, G. Reifenberger, H. W. Muller, K. Zilles, H. H. Coenen, and K. J. Langen, "O-(2-[18F]fluoroethyl)-L-tyrosine PET combined with MRI improves the diagnostic assessment of cerebral gliomas," *Brain* **128**, 678–687 (2005).

⁸ R. R. Raylman, S. Majewski, S. K. Lemieux, S. S. Velan, B. Kross, V. Popov, M. F. Smith, A. G. Weisenberger, C. Zorn, and G. D. Marano, "Simultaneous MRI and PET imaging of a rat brain," *Phys. Med. Biol.* **51**, 6371–6379 (2006).

⁹ Y. P. Shao, S. R. Cherry, K. Farahani, K. Meadors, S. Siegel, R. W. Silverman, and P. K. Marsden, "Simultaneous PET and MR imaging," *Phys. Med. Biol.* **42**, 1965–1970 (1997).

¹⁰ J. E. Mackewn, D. Strul, W. A. Hallett, P. Halsted, R. A. Page, S. F. Keevil, S. C. R. Williams, S. R. Cherry, and P. K. Marsden, "Design and development of an MR-compatible PET scanner for imaging small animals," *IEEE Trans. Nucl. Sci.* **52**, 1376–1380 (2005).

¹¹ S. Yamamoto, M. Imaizumi, Y. Kanai, M. Tatsumi, M. Aoki, E. Sugiyama, M. Kawakami, E. Shimosegawa, and J. Hatazawa, "Design and performance from an integrated PET/MRI system for small animals," *Ann. Nucl. Med.* **24**, 89–98 (2010).

¹² C. Woody, D. Schlyer, P. Vaska, D. Tomasi, S. Solis-Najera, W. Rooney, J. F. Pratte, S. Junnarkar, S. Stoll, Z. Master, M. Purschke, S. J. Park, S. Southekal, A. Kriplani, S. Krishnamoorthy, S. Maramraju, P. O'Connor, and V. Radeka, "Preliminary studies of a simultaneous PET/MRI scanner based on the RatCAP small animal tomograph," *Nucl. Instrum. Methods Phys. Res. A* **571**, 102–105 (2007).

¹³ M. S. Judenhofer, C. Catana, B. K. Swann, S. B. Siegel, W. I. Jung, R. E. Nutt, S. R. Cherry, C. D. Claussen, and B. J. Pichler, "PET/MR images acquired with a compact MR-compatible PET detector in a 7-T magnet," *Radiology* **244**, 807–814 (2007).

¹⁴ H. P. W. Schlemmer, B. J. Pichler, M. Schmand, Z. Burbar, C. Michel, R. Ladebeck, K. Jattke, D. Townsend, C. Nahmias, P. K. Jacob, W. D. Heiss, and C. D. Claussen, "Simultaneous MR/PET imaging of the human brain: Feasibility study," *Radiology* **248**, 1028–1035 (2008).

¹⁵ W. R. Leo, *Techniques for Nuclear and Particle Physics Experiments: A How-To Approach* (Springer, New York, 1994), Chap. 10, pp. 244–245.

¹⁶ J. F. Schenck, "The role of magnetic susceptibility in magnetic resonance imaging: MRI magnetic compatibility of the first and second kinds," *Med. Phys.* **23**, 815–850 (1996).

¹⁷ S. Yamamoto, K. Kuroda, and M. Senda, "Scintillator selection for MR-compatible gamma detectors," *IEEE Trans. Nucl. Sci.* **50**, 1683–1685 (2003).

¹⁸ P. J. Hughes, D. Herbert, A. Stewart, and J. C. Jackson, "Tiled silicon photomultipliers for large-area low-light sensing applications," *Proc. SPIE* **6471**, 647112.1–647112.8 (2007).

¹⁹ J. C. Jackson, "Silicon photomultiplier detectors for low light detection," *Photonics Spectra* **41**, 64–66 (2007).

²⁰ M. Streun, G. Brandenburg, H. Larue, E. Zimmermann, K. Ziemons, and F. Halling, "Coincidence detection by digital processing of free-running sampled pulses," *Nucl. Instrum. Methods Phys. Res. A* **487**, 530–534 (2002).

²¹ V. Radeka and P. O'Conner, "Integrated circuit front ends for nuclear pulse processing," in Proceedings of the IEEE Nuclear Science Symposium and Medical Imaging Conference Short Course, 2007.

²² P. D. Olcott, H. Peng, and C. S. Levin, "Novel electro-optical coupling technique for magnetic resonance-compatible positron emission tomography detectors," *Mol. Imaging* **8**, 74–86 (2009).

²³ D. R. Schaart, H. T. van Dam, S. Seifert, R. Vinke, P. Dendooven, H. Lohner, and F. J. Beekman, "A novel, SiPM-array-based, monolithic scintillator detector for PET," *Phys. Med. Biol.* **54**, 3501–3512 (2009).

²⁴ G. Brianti, "Distortion of fast pulses in coaxial cables numerical analysis

- and applications,” CERN Report No. 65-10 (MSC Division, 1965).
- ²⁵P. Despres, E. W. Izaguirre, S. Liu, L. J. Cirignano, H. Kim, M. F. Wendland, K. S. Shah, and B. H. Hasegawa, “Evaluation of a MR-compatible CZT detector,” *IEEE Nuclear Science Symposium Conference Record* **6**, 4324–4326 (2007).
- ²⁶C. Catana, D. Procissi, Y. B. Wu, M. S. Judenhofer, J. Y. Qi, B. J. Pichler, R. E. Jacobs, and S. R. Cherry, “Simultaneous in vivo positron emission tomography and magnetic resonance imaging,” *Proc. Natl. Acad. Sci. U.S.A.* **105**, 3705–3710 (2008).
- ²⁷A. Kolb, E. Lorenz, M. S. Judenhofer, D. Renker, K. Lankes, and B. J. Pichler, “Evaluation of Geiger-mode APDs for PET block detector designs,” *Phys. Med. Biol.* **55**, 1815–1832 (2010).